Multibeam fluorescence diffuse optical tomography using upconverting nanoparticles

Haichun Liu,* Can T. Xu, and Stefan Andersson-Engels

Department of Physics, Lund University, P.O. Box 118, S-221 00 Lund, Sweden
**Corresponding author: haichun.liu@fysik.lth.se*

Received November 2, 2009; revised December 18, 2009; accepted January 11, 2010;
posted January 12, 2010 (Doc. ID 119223); published February 25, 2010

Fluorescence diffuse optical tomography (FDOT) is a biomedical imaging modality that can be used for localization and quantification of fluorescent molecules inside turbid media. In this ill-posed problem, the reconstruction quality is directly determined by the amount and quality of the information obtained from the boundary measurements. Regularly, more information can be obtained by increasing the number of excitation positions in an FDOT system. However, the maximum number of excitation positions is limited by the finite size of the excitation beam. In the present work, we demonstrate a method in FDOT to exploit the unique nonlinear power dependence of upconverting nanoparticles to further increase the amount of information in a raster-scanning setup by including excitation with two beams simultaneously. We show that the additional information can be used to obtain more accurate reconstructions. © 2010 Optical Society of America

OCIS codes: 170.3880, 170.6960, 170.7050, 100.3190.

Fluorescence diffuse optical tomography (FDOT) is a relatively new modality that seeks to reconstruct the spatial distribution of fluorescent probes inside turbid materials [1]. As an imaging tool, it has good prospects in biomedical studies to image, for example, tumors [2], proteases [3], and drug effects [4].

FDOT is a numerically very ill-posed problem. In this problem, the quality of the reconstructions for the fluorescent target is directly determined by the amount and quality of fluorescence information obtained from boundary measurements [5]. Instrumental noise and tissue autofluorescence are the main perturbations of the measurements, resulting in poor signal quality, and can cause severe artifacts in the reconstructed results [6]. To overcome this, one could, for example, employ low-noise equipment, use background subtraction [7], or use spectral unmixing [8]. However, such methods cannot resolve all problems, since they essentially are only utilizing the present information in a better way rather than adding new constraints for the reconstructions, i.e., adding new independent information, which is critical to improve the quality of the reconstructions.

In a noncontact CCD-based FDOT system, one preferred way to gain more information is by increasing the number of excitation positions [9]. However, in order to keep the intensity of the excitation beam within reasonable levels, there is a limit on the minimum size of the excitation beam. This implies a practical upper limit to the highest excitation-position density, since distinct, i.e., nonoverlapping, excitation positions are desired in the reconstructions. It is also possible to employ an anatomical imaging modality such as magnetic-resonance imaging to provide *a priori* structural information [10]. However, this is at the cost of significantly increased complexity and reduced flexibility of the system.

Upconverting nanoparticles have been proposed as fluorophores in biomedical imaging [11,12] as well as in FDOT [13]. These nanoparticles can emit anti-Stokes shifted light when excited at 980 nm [14], which enables the signal to be detected in an autofluorescence-free environment [15]. This leads to a significant reduction of artifacts in the reconstructions. In addition, owing to the quadratic power dependence of the nanoparticles, the reconstructions are more sharply defined compared with the reconstructions of a linear fluorophore [13].

In this Letter, we present an approach to exploit the quadratic power dependence of upconverting nanoparticles to gain additional information by utilizing two beams simultaneously for excitation in FDOT. The effect of the images taken with dual-beam excitation (named type-D images) on the reconstructions of the nanoparticle number density distribution, n, is demonstrated. In addition, comparisons of reconstructed results between the linear rhodamine 6G and the quadratic upconverting nanoparticles are made.

The excitation and emission fields can be modeled by two coupled diffusion equations [13]. For quadratic fluorophores, the fluorescence signal detected at a fixed detector position under excitation of the kth beam, Γ_k, can be described by the forward model

$$\Gamma_k = \sum_{i=1}^{N} U_{\mathrm{f}}^{*}(\mathbf{r}_{\mathrm{d}}, \mathbf{r}_i) n(\mathbf{r}_i) [U_{\mathrm{e}}(\mathbf{r}_{\mathrm{s}_k}, \mathbf{r}_i)]^2 \Delta V_i, \qquad (1)$$

where N denotes the number of voxels; $\mathbf{r}_{\mathrm{s,d},i}$ denotes the coordinates for source, detector, and voxel, respectively; and ΔV_i is the volume of voxel i. The forward solution of the excitation light is represented by $[U_{\mathrm{e}}(\mathbf{r}_{\mathrm{s}_k}, \mathbf{r}_i)]^2$, while the adjoint solution to the forward fluorescence problem is represented by $U_{\mathrm{f}}^{*}(\mathbf{r}_{\mathrm{d}}, \mathbf{r}_i)$. When exciting the medium using two beams simultaneously, the detected signal is given by

0146-9592/10/050718-3/$15.00

$$\Gamma_{k\&j} = \sum_{i=1}^{N} U_f^*(\mathbf{r}_d,\mathbf{r}_i) n(\mathbf{r}_i)[U_e(\mathbf{r}_{s_k},\mathbf{r}_i) + U_e(\mathbf{r}_{s_j},\mathbf{r}_i)]^2 \Delta V_i$$
$$= 2\sum_{i=1}^{N} U_f^*(\mathbf{r}_d,\mathbf{r}_i) n(\mathbf{r}_i) U_e(\mathbf{r}_{s_k},\mathbf{r}_i) U_e(\mathbf{r}_{s_j},\mathbf{r}_i) \Delta V_i + \Gamma_k + \Gamma_j, \quad (2)$$

which reveals the involvement of cross terms. In a raster-scanning setup, if two images are taken sequentially with one excitation beam scanning over two positions (named type-S images), and a third image is taken with dual-beam excitation (type-D) above the previous two positions, the involvement of cross terms implies that the type-D image cannot be obtained by any mathematical manipulation from the existing type-S images, indicating that it is independent and contains additional information. However, for linear fluorophores, e.g., rhodamine 6G, the type-D image is only a linear combination of the existing type-S images and will not add more constraints for the inverse problem. For nonlinear fluorophores, it is obvious that Eq. (2) can be generalized to include more simultaneous excitation beams.

The significance of the measurements with dual-beam excitation in the reconstructions was confirmed by the singular-value analysis of the weight matrix, W, whose elements are given by [13]

$$W_{(s,d),i} = U_f^*(\mathbf{r}_d,\mathbf{r}_i)[U_e(\mathbf{r}_s,\mathbf{r}_i)]^\gamma \Delta V_i, \quad (3)$$

with $\gamma=1$ for linear fluorophores and $\gamma=2$ for quadratic fluorophores. Calculations were performed using the NIRFAST package implementing the finite-element method [16]. W was factorized according to

$$W = U\Sigma V^*, \quad (4)$$

where U and V are unitary matrices containing the left and right singular vectors of W, respectively, and Σ is a diagonal matrix containing the singular values of W. The column space of V is spanned by the image-space modes, while the column space of U is spanned by the detection-space modes. The singular values of W denote how effectively a given image-space mode can be detected by an experimental setup [17].

Figure 1 shows the normalized singular-value distribution of W. For clarity, only every second singular value is shown. The circle and plus signs represent the linear fluorophore, the former for the single-beam excitation, while the latter for the combined single-beam excitation and dual-beam excitation. As seen, the normalized intensities of the additional singular values due to dual-beam excitation have dropped to machine precision, which indicates that the measurements with dual-beam excitation will not alleviate the ill-posedness of FDOT. In other words, the type-D images cannot provide more information than the existing type-S images. Hence, it will not improve the quality of the reconstructions. However, for the quadratic fluorophore (denoted by asterisk and dot signs in Fig. 1), the intensities of the additional singular values are still significant. This implies that type-D images will contribute to the quality of the reconstructions.

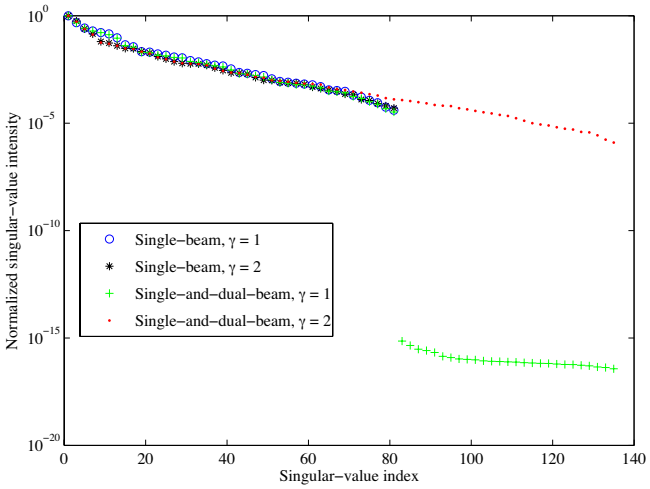

Fig. 1. (Color online) Singular-value distribution of W.

The experiments were carried out in a gelatin phantom with optical properties of $\mu_a=0.29\ \mathrm{cm}^{-1}$ and $\mu_s'=10.0\ \mathrm{cm}^{-1}$ at 660 nm, measured with a time-of-flight spectroscopy system [18]. Two glass tubes with inner diameters of 2.4 mm, filled with aqueous solutions of rhodamine 6G ($c=0.1\ \mu\mathrm{M}$) and ultrasound-agitated dimethyl sulfoxide colloidal of $NaYF_4:Yb^{3+}/Tm^{3+}$ nanoparticles ($c=1$ wt%), respectively, were used to simulate the fluorescent lesions. The spot sizes of the lasers were 2.6 mm in diameter, which gave optical power densities of 480 $\mathrm{mW/cm^2}$ for the 980 nm laser and 85 $\mathrm{mW/cm^2}$ for the 532 nm laser, well below the damage thresholds of continuous human-skin exposure. The experimental setup and corresponding running parameters were similar with those used in our previous work [13]. Owing to the limited area of the phantom under investigation, only nine excitation positions (3×3 grid) were used in the present work. The separation of two nearest-neighboring positions was 3.5 mm. During the experiments, a single excitation beam was first used to scan over the 3×3 grid, and one image was captured for each scanned position by a CCD camera. In the next step, two excitation beams, located at two nearest-neighboring sites of the same grid, were simultaneously employed to illuminate the phantom, giving six extra type-D images.

Figure 2 shows the three-dimensional rendering of the reconstructed upconverting nanoparticles. The cylinders in the subfigures are identical and represent the true fluorescent lesions. In the reconstruction of Fig. 2(a), only type-S images were used. As can be seen, the shape of the fluorescent lesion is overestimated. This overestimation may be explained by the ill-posedness of the inverse problem. When adding type-D images, the reconstruction of the fluorescent lesion shape is improved remarkably, as shown in Fig. 2(b). In order to emphasize the difference between the two reconstructions, cross-sectional slices of the reconstructed relative fluorophore distribution are shown in Fig. 3. Although the depth is relatively

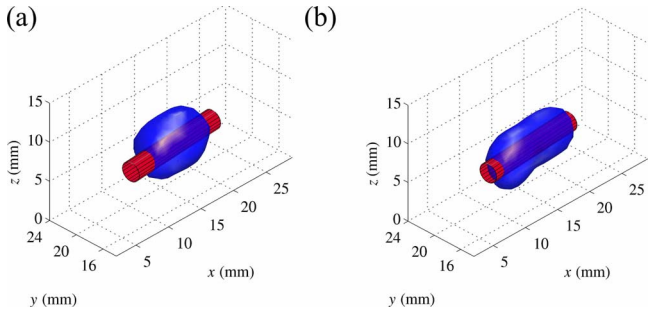

Fig. 2. (Color online) Three-dimensional reconstruction of upconverting nanoparticles. (a) Reconstruction using only type-S images. (b) Reconstruction using the combined data from type-S and type-D images.

well reconstructed at the center of the fluorescent lesion (represented by the circles) for both reconstructions, the reconstructed fluorescent lesion is more confined for the case of using both type-S and type-D images. This result confirms that the images of type D indeed contribute to the inverse problem and lead to better reconstructions for the quadratic upconverting nanoparticles. The corresponding reconstructions for the linear rhodamine 6G were also carried out, whose cross-sectional slices are presented in Fig. 4. Compared with the results for the nanoparticles, the reconstructions for rhodamine 6G do not benefit from adding the type-D images, which is in agreement with the theory. The true depth of the fluorescent lesion is also poorly reconstructed.

In summary, based on previous work regarding the employment of upconverting nanoparticles in FDOT, we propose and demonstrate an additional unique advantage of the nonlinear power dependence of upconverting nanoparticles. This advantage enables the possibility to obtain additional information for the inverse problem by using images taken with two or more excitation beams simultaneously. We found that this resulted in improved reconstructions. The same advantage could not be found when using linear fluorophores, e.g., rhodamine 6G.

This work was supported by a Swedish Research Council grant (VR 2007-4214) and a Linnaeus grant for the Lund Laser Centre. The authors thank Prof. Zhiguo Zhang and his group from the Harbin Institute of Technology and Dr. Gabriel Somesfalean for their collaboration work.

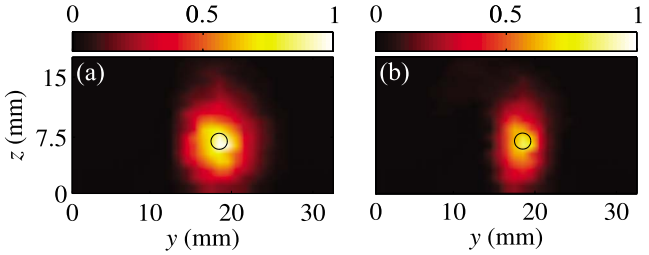

Fig. 3. (Color online) Cross-sectional slices of the reconstructed relative nanoparticle distribution at $x=17$ mm. (a) Reconstruction with only type-S images. (b) Reconstruction with both type-S and type-D images.

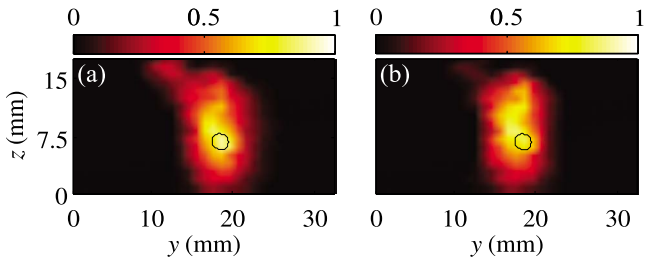

Fig. 4. (Color online) Cross-sectional slices of the reconstructed relative rhodamine 6G distribution at $x=17$ mm. (a) Reconstruction with only type-S images. (b) Reconstruction with both type-S and type-D images.

References

1. A. Hielscher, Curr. Opin. Biotechnol. **16**, 79 (2005).
2. A. Corlu, R. Choe, T. Durduran, M. A. Rosen, M. Schweiger, S. R. Arridge, M. D. Schnall, and A. G. Yodh, Opt. Express **15**, 6696 (2007).
3. V. Ntziachristos, C.-H. Tung, C. Bremer, and R. Weissleder, Nat. Med. **8**, 757 (2002).
4. V. Ntziachristos, E. A. Schellenberger, J. Ripoll, D. Yessayan, E. Graves, A. Bogdanov, L. Josephson, and R. Weissleder, Proc. Natl. Acad. Sci. USA **101**, 12294 (2004).
5. S. R. Arridge, Inverse Probl. **15**, R41 (1999).
6. A. Soubret and V. Ntziachristos, Phys. Med. Biol. **51**, 3983 (2006).
7. D. C. Comsa, T. J. Farrell, and M. S. Patterson, Phys. Med. Biol. **53**, 5797 (2008).
8. J. R. Mansfield, K. W. Gossage, C. C. Hoyt, and R. M. Levenson, J. Biomed. Opt. **10**, 041207 (2005).
9. G. Y. Panasyuk, Z.-M. Wang, J. C. Schotland, and V. A. Markel, Opt. Lett. **33**, 1744 (2008).
10. S. C. Davis, B. W. Pogue, R. Springett, C. Leussler, P. Mazurkewitz, S. B. Tuttle, S. L. Gibbs-Strauss, S. S. Jiang, H. Dehghani, and K. D. Paulsen, Rev. Sci. Instrum. **79**, 064302 (2008).
11. S. F. Lim, R. Riehn, W. S. Ryu, N. Khanarian, C.-K. Tung, D. Tank, and R. H. Austin, Nano Lett. **6**, 169 (2006).
12. C. Vinegoni, D. Razansky, S. A. Hilderbrand, F. Shao, V. Ntziachristos, and R. Weissleder, Opt. Lett. **34**, 2566 (2009).
13. C. T. Xu, J. Axelsson, and S. Andersson-Engels, Appl. Phys. Lett. **94**, 251107 (2009).
14. H. J. Liang, G. Y. Chen, L. Li, Y. Liu, F. Qin, and Z. G. Zhang, Opt. Commun. **282**, 3028 (2009).
15. C. T. Xu, N. Svensson, J. Axelsson, P. Svenmarker, G. Somesfalean, G. Y. Chen, H. J. Liang, H. C. Liu, Z. G. Zhang, and S. Andersson-Engels, Appl. Phys. Lett. **93**, 171103 (2008).
16. H. Dehghani, M. E. Eames, P. K. Yalavarthy, S. C. Davis, S. Srinivasan, C. M. Carpenter, B. W. Pogue, and K. D. Paulsen, Commun. Numer. Methods Eng. **25**, 711 (2009).
17. J. P. Culver, V. Ntziachristos, M. J. Holboke, and A. G. Yodh, Opt. Lett. **26**, 701 (2001).
18. E. Alerstam, S. Andersson-Engels, and T. Svensson, J. Biomed. Opt. **13**, 041304 (2008).